ELSEVIER

Journal of Magnetism and Magnetic Materials 206 (1999) 93–105

Journal of magnetism and magnetic materials

www.elsevier.com/locate/jmmm

Microwave polarizability of ferrite particles with non-uniform magnetization

S. Labbé, P.-Y. Bertin*

Office National d'Etudes et de Recherches Aérospatiales, BP 72, 92322 Châtillon Cédex, France

Received 3 July 1998; received in revised form 20 July 1999

Abstract

The microwave permeability of composites made of ferrite particles in a non-magnetic matrix is affected by particle shape and size. To account for the second effect, we have developed a micromagnetic model for calculating the microwave polarizability of a particle with non-uniform magnetization. This model is described in detail: a generalized demagnetizing operator associated with the equilibrium magnetic configuration inside the particle is introduced; the polarizability is defined as the perturbation of this configuration by the external magnetic excitation; the permeability of a macroscopic sample is calculated using a space averaging procedure. The numerical methods are introduced and results for two systems are discussed: domain modes in thin films and ferrite composites with planar anisotropy.

PACS: 75.30.C; 75.50.G; 75.60.C; 75.70.K

Keywords: Ferrite; Microwave; Anisotropy – planar; Composite material; Micromagnetism; Magnetic particle; Magnetic film

1. Introduction

Microwave permeability spectra in zero-field of soft ferrimagnets reflect the magnetic domain structure of the material through wall relaxation and high frequency losses above the gyromagnetic resonance [1]. Models considering the response of an infinite domain arrangement lead to a quantitative interpretation of the high frequency spectrum for ceramics [2,3] and films [4].

However, finite size effects frequently occur in magnetic materials and modify greatly the microwave response. This is the case in ceramics with the grain size dependence of wall relaxation [5]. Another finite size effect is observed in composites made of magnetic particles in a non-magnetic matrix: the intrinsic susceptibility of the material in particulate form is different from that in ceramic form and varies with particle size [6]. Interpretation of these effects requires the introduction of the material's microstructure. In ceramics, a specific dynamics for domain walls in which the grain size is introduced [5] is considered. In composites, the particle size affects the magnetic configuration inside the particles due to the exchange interaction. This is the reason why small sized particles have a non-zero remanent magnetization: the magnetic interaction between these

* Corresponding author. Tel.: + 33-1-46-73-45-03; fax: + 33-1-46-73-48-24.

E-mail address: bertin@onera.fr (P.-Y. Bertin)

0304-8853/99/$ - see front matter
PII: S0304-8853(99)00537-5

monodomain particles produces an aggregate morphology of the powder; this specific morphology changes the microwave response of fine powders compared to polydomain particles with zero remanent magnetization.

The quantitative interpretation of the particle size effect in composites requires the description of how this parameter affects the magnetic configuration inside the composite. Calculating magnetic configurations involves the Landau–Lifshitz equation for magnetization dynamics: it is called micromagnetics and is done numerically most of the time [7]. Micromagnetics is used to investigate both static and dynamic properties such as magnetization reversal in particles [8], remanence in nanocomposite magnets [9] and motion of domain walls in garnet films [10]. The magnetic configuration is defined at an intermediate lengthscale (0.01 μm), between macroscopic (sample size) and microscopic (atomic) lengthscales.

A micromagnetic model for composites microwave permeability was first developed in the case of monodomain particles (of size of the order of 0.01 μm): the intermediate lengthscale in this case is the particle size and the magnetization is discrete, each particle carrying a magnetic moment of given amplitude. In an aggregate with a given morphology, the relative orientation of the particle's moments depends on the magnetocrystalline anisotropy of individual particles and on the magnetic dipolar interaction between particles. Considering different aggregate morphologies, we were able to account for the permeability spectra measured on different iron composites [11,12].

In this paper, we turn to composites made of insulating polydomain particles (a few micrometers in size, with a non-uniform magnetization): at the micromagnetic lengthscale of 0.01 μm, magnetization inside one particle is continuous and its configuration depends on the magnetocrystalline anisotropy, demagnetizing field and exchange interaction in the finite three-dimensional volume of the particle. This kind of numerical simulation requires a careful space discretization of the demagnetizing field inside one particle (dipolar interactions in a continuous medium) and appropriate numerical methods [13,14]. The aim of this paper is to make a general presentation of the model and show how it can account for particle size effects.[1]

In Section 1, the concepts and notations are introduced by presenting the conventional model for calculating a composite's permeability in the low concentration regime. The micromagnetic model, relying on the definition of a particle's polarizability, is presented in Section 3. In Section 4, results of preliminary simulations using specific numerical methods are presented in two special cases: finite portions of thin films featuring domain modes and ferrite particles with planar anisotropy.

2. Conventional model

In the microwave range (100 MHz–10 GHz), the permittivity ε and permeability μ are defined for a homogeneous composite sample, with a microstructure lengthscale (particle size: <100 μm) small compared to the wavelength of the material (of the order of $1–10^{-2}$ m for insulating particles). The propagating electromagnetic wave acts as both electric and magnetic harmonic excitations, producing electric and magnetic responses. At the micromagnetic lengthscale of 0.01 μm, the excitations are independent of each other (quasi-stationary approximation). It is supposed that the magnetic material's response to these two excitations can be decomposed into two independent components: one related to the electric field and given by electrostatics; the other to the magnetic field and given by magnetostatics.

The permeability μ is related to the induced microscopic magnetic moments. Let $\boldsymbol{H}_{\text{ext}}$ be the external magnetic excitation seen by a given particle and $\boldsymbol{p}$, the magnetic moment induced in that particle by $\boldsymbol{H}_{\text{ext}}$. The particle's polarizability α is

[1] A particle size dependence of the permeability is observed on composites made of conducting particles at frequencies where the skin depth (~ 1 μm for a metal in the microwave range) is of the order of particle size. Although contributing to the magnetic polarizability, this electrical screening effect is not directly related to the magnetic configuration inside the particles. We deal here with insulating particles.

then defined by

$$\boldsymbol{p} = \alpha \boldsymbol{H}_{\text{ext}} V, \tag{1}$$

where V is the particle's volume. Inside this particle, $\boldsymbol{p}$ builds up from the induced magnetization density $\boldsymbol{M}$ due to the material's susceptibility χ to the internal excitation $\boldsymbol{H}$:

$$\boldsymbol{M} = \chi \boldsymbol{H} \tag{2}$$

$\boldsymbol{H}$ obeys the equations of magnetostatics:

$$\text{div}\, \boldsymbol{B}(\boldsymbol{x}, t) = 0 \quad \text{rot}\, \boldsymbol{H}(\boldsymbol{x}, t) = 0,$$

$$\boldsymbol{B}(\boldsymbol{x}, t) = \mu_0(\boldsymbol{H}(\boldsymbol{x}, t) + \boldsymbol{M}(\boldsymbol{x}, t)), \tag{3}$$

where $\boldsymbol{B}$ is the magnetic field and μ_0, the permeability in vacuum. In the case of a spherical particle of uniform susceptibility χ surrounded by vacuum, these equations give a uniform $\boldsymbol{M}$ and $\boldsymbol{H}$ inside the particle [15]:

$$\boldsymbol{H} = -\frac{\boldsymbol{M}}{3} + \boldsymbol{H}_{\text{ext}}, \tag{4}$$

$$\boldsymbol{M} = \frac{\chi}{1 + \chi/3} \boldsymbol{H}_{\text{ext}}. \tag{5}$$

Since $\boldsymbol{M}$ is uniform, $\boldsymbol{p} = \boldsymbol{M}V$ and the polarizability α is given by

$$\alpha = \frac{\chi}{1 + \chi/3}, \tag{6}$$

where $\frac{1}{3}$ is the sphere's demagnetizing factor. Outside the particle, $\boldsymbol{M} = 0$ (non-magnetic matrix). The SI units for $\boldsymbol{M}$, $\boldsymbol{H}$ and $\boldsymbol{H}_{\text{ext}}$ are A m^{-1}; $\boldsymbol{p}$ is in A m^2; α and χ are dimensionless; μ is in H m^{-1} (in vacuum, $\mu_0 = 4\pi \times 10^{-7}$ H m^{-1}).

Complex particle shapes (e.g. rectangular prism) can be approximated by an ellipsoid. The polarizability along one principal axis of an ellipsoid is given by

$$\alpha_{kk} = \chi/(1 + N_k \chi), \tag{7}$$

where $\{N_k\}$ $(k = x, y, z)$ are the demagnetizing factors. This formula can be extended to arbitrary shapes considering N_k as effective demagnetizing factors, fixed by the particle's aspect ratio. Thus, α depends on both particle shape (N_k) and intrinsic material properties (χ). Since the equations of magnetostatics involve no time derivative, formula (7) holds for a harmonic excitation: χ and α are then complex numbers. The induced moment inside the particle generates a multipolar field (purely dipolar in the case of a sphere) outside the particle which influences neighboring particles inside the composite.

These interactions between particles can be represented by a modification of the external excitation seen by a given particle (mean field approximation). $\boldsymbol{H}_{\text{ext}}$ is then defined as the magnetic excitation at the microscopic scale that would exist in the composite if that particle were absent: it is generated by the electromagnetic wave and all the other particles. At sufficiently low concentration, the field generated by the other particles can be neglected; $\boldsymbol{H}_{\text{ext}}$ is then the truly external harmonic excitation, produced by the electromagnetic wave alone. Due to the quasi-stationary approximation, this excitation is uniform at the lengthscale of particle size. Averaging $\boldsymbol{M}$ over a large volume compared to particle size yields the average permeability of the composite (valid in the low concentration regime):

$$(\mu - \mu_0)/\mu_0 \sim C\alpha, \tag{8}$$

where C is the volume fraction of particles $(0 < C < 1)$.

Formula (8) is in fact valid in a large concentration range. Experiment and theoretical arguments based on the effective medium theory [16] give the low concentration regime at $C < 30\%$. In the case of polydomain particles, this can be understood from the low remanent magnetic moment of each particle: particle interactions are weak and the composite's permeability is dominated by the polarizability of individual particles. For concentrations up to 30%, the composites permeability spectrum is simply proportional to C and gives the particles average polarizability spectrum.

3. Micromagnetic model

The above conventional model can account for particle shape effects through dimensionless demagnetizing factors as in Eq. (7). In this model,

particle size effects can only be introduced through χ. If χ reflects the magnetic configuration inside a particle according to its size, it is not representative of the infinite material anymore, as postulated originally in the conventional model. The argument can still be made valid by considering the macroscopic susceptibility χ of the composite for an arbitrarily chosen domain structure inside the particles. However, the particle size still does not appear explicitly. The influence of this parameter can be made explicit by calculating the magnetic configuration inside a particle of given shape and size and by defining its polarizability: it is a micromagnetic model.

In this model, a polydomain particle is seen as a three-dimensional, bounded magnetic medium Ω of homogeneous composition, surrounded by vacuum. The magnetic configuration is defined in the entire space, denoted by $\Re$, with the following constraint:

$$|\boldsymbol{M}(\boldsymbol{x}, t)| = M_S(T) \quad \text{for } \boldsymbol{x} \text{ in } \Omega, \tag{9}$$

$$|\boldsymbol{M}(\boldsymbol{x}, t)| = 0 \quad \text{for } \boldsymbol{x} \text{ in } \Re/\Omega,$$

where $M_S(T)$ is the non-vanishing thermodynamic saturation magnetization at temperature T for the given composition. For a small amplitude electromagnetic wave, the particle's response to $\boldsymbol{H}_{ext}$ is seen as the perturbation of an equilibrium configuration $\{\boldsymbol{M}_0\}$. Due to the magnetic moments dynamics (see Eq. (20) below), $\{\boldsymbol{M}_0\}$ must satisfy at all points:

$$\boldsymbol{M}_0(\boldsymbol{x}) \wedge \boldsymbol{H}(x) = 0, \tag{10}$$

where $\boldsymbol{H}$ is the excitation inside the particle in the absence of $\boldsymbol{H}_{ext}$. As expressed by Eq. (5) in the case of a demagnetized particle with uniform susceptibility χ, the perturbation of $\{\boldsymbol{M}_0\}$ produced by $\boldsymbol{H}_{ext}$ defines the particle's polarizability α. Thus, the micromagnetic model is applied by performing a two steps calculation: the first one yields $\{\boldsymbol{M}_0\}$ and the second one $\{\delta\boldsymbol{M}\}$; the perturbations in the vicinity of $\{\boldsymbol{M}_0\}$ due to $\boldsymbol{H}_{ext}$. In order to calculate the internal micromagnetic excitation $\boldsymbol{H}$ involved in Eq. (10), we introduce the generalized demagnetizing operator.

3.1. Generalized demagnetizing operator

The internal excitation $\boldsymbol{H}$ is defined from the energy density $E(\boldsymbol{x}, t)$ (in $\mathrm{J\,m^{-3}}$) associated with a given magnetic configuration $\{\boldsymbol{M}\}$:

$$\boldsymbol{H}(\boldsymbol{x}, t) = -\partial E/\partial(\mu_0 \boldsymbol{M}). \tag{11}$$

E involves four contributions giving rise to four terms in $\boldsymbol{H}$:

$$E(\{\boldsymbol{M}\}) = E_{ext} + E_d + E_e + E_a, \tag{12}$$

$$\boldsymbol{H}(\boldsymbol{x}, t) = \boldsymbol{H}_{ext} + \boldsymbol{H}_d + \boldsymbol{H}_e + \boldsymbol{H}_a. \tag{13}$$

$\boldsymbol{H}_{ext}$ is the external excitation produced by the electromagnetic wave. $\boldsymbol{H}_d$ is the demagnetizing field obeying Eq. (3) as in the conventional model. The two other contributions stem from the ferrimagnetic character of the material. The exchange interaction (responsible for atomic moments alignment from which $\boldsymbol{M}$ builds up in a ferromagnetic medium) is given by

$$E_e = A|\nabla \boldsymbol{M}|^2/M_S^2$$

$$\boldsymbol{H}_e(\boldsymbol{x}, t) = (2A/\mu_0 M_S^2)\Delta \boldsymbol{M}(\boldsymbol{x}, t) \tag{14}$$

and the magnetocrystalline anisotropy, by:

$$E_a = K[1 - (\boldsymbol{M}(\boldsymbol{x}, t)\cdot \boldsymbol{u})^2/M_S^2],$$

$$\boldsymbol{H}_a(\boldsymbol{x}, t) = (2K/\mu_0 M_S^2)\varphi(\boldsymbol{M}(\boldsymbol{x}, t)), \tag{15}$$

$$\varphi(\boldsymbol{M}(\boldsymbol{x}, t)) = [(\boldsymbol{M}(\boldsymbol{x}, t)\cdot \boldsymbol{u})\boldsymbol{u} - \boldsymbol{M}(\boldsymbol{x}, t)] \quad (K > 0),$$

$$= (\boldsymbol{M}(\boldsymbol{x}, t)\boldsymbol{u})\cdot \boldsymbol{u}, \quad (K < 0).$$

A is the exchange constant (expressed in $\mathrm{J\,m^{-1}}$), K the quadratic uniaxial[2] anisotropy constant (expressed in $\mathrm{J\,m^{-3}}$) and $\boldsymbol{u}$, the anisotropy direction (unit vector).

Among the three contributions, the demagnetizing one has the peculiarity of being non-local. The general solution for $\boldsymbol{H}_d(\boldsymbol{x}, t)$ of Eq. (3) is [15]

$$\boldsymbol{H}_d(\boldsymbol{x}, t) = \frac{1}{4\pi}\,\mathrm{grad\ div} \int_{\Re} [\boldsymbol{M}(\boldsymbol{x}', t)/|\boldsymbol{x} - \boldsymbol{x}'|]dx' \tag{16}$$

[2] As a first approximation, we ignore anisotropy orders higher than 2 (uniaxial, hexagonal or cubic) which lead to a nonlinear relation between $\boldsymbol{H}_a$ and $\boldsymbol{M}$.

$\boldsymbol{H}_d(\boldsymbol{x}, t)$ is not only determined by $\boldsymbol{M}(\boldsymbol{x}, t)$ but by the entire magnetic configuration $\{\boldsymbol{M}\}$. In the same way, the demagnetizing field distribution is noted between braces and linear relation (16) becomes

$$\{\boldsymbol{H}_d\} = -\boldsymbol{N}\{\boldsymbol{M}\}, \tag{17}$$

where $\boldsymbol{N}$ is a linear operator, which we call the demagnetizing operator; $-\boldsymbol{N}$ acts on $\{\boldsymbol{M}\}$ and yields the demagnetizing field $\{\boldsymbol{H}_d\}$ in the entire volume Ω (even outside). Its eigenvalues are between 0 and 1: thus $-\boldsymbol{N}$ is negative [17]. Similarly, the two operators acting on $\{\boldsymbol{M}\}$ and giving $\{\boldsymbol{H}_e\}$ and $\{\boldsymbol{H}_a\}$ as defined by Eqs. (14) and (15) are also negative linear operators. Introducing the generalized demagnetizing operator $\tilde{\boldsymbol{N}}$, expression (13) can be written as

$$\{\boldsymbol{H}\} = -\tilde{\boldsymbol{N}}\{\boldsymbol{M}\} + \{\boldsymbol{H}_{ext}\}, \tag{18}$$

$$\tilde{\boldsymbol{N}} = \boldsymbol{N} - 2(A/\mu_0 M_S^2)\Delta - 2(K/\mu_0 M_S^2)\varphi,$$

where $\{\boldsymbol{H}\}$ is the total (in general non-uniform) internal excitation and $\{\boldsymbol{H}_{ext}\}$, the external excitation, uniform over Ω. This expression generalizes Eq. (4). In the special case of a demagnetized sphere with uniform susceptibility, without exchange and anisotropy, $\tilde{\boldsymbol{N}}$ reduces to $\boldsymbol{N}$ and is diagonal (multiplication by $\frac{1}{3}$).

The generalized demagnetizing operator $\tilde{\boldsymbol{N}}$ allows an operational definition of the equilibrium configuration $\{\boldsymbol{M}_0\}$. $\boldsymbol{H}_{ext}$ being treated as a perturbation of $\{\boldsymbol{M}_0\}$, expression (10) becomes:

$$\boldsymbol{M}_0(\boldsymbol{x}) \wedge \tilde{\boldsymbol{N}}\{\boldsymbol{M}_0\} = 0. \tag{19}$$

The fact that the solution to this equation is not unique accounts for the dependence $\{\boldsymbol{M}_0\}$ with history (hysterisis phenomena) or, in numerical simulations, with the chosen initial configuration $\{\boldsymbol{M}_i\}$.

3.2. Micromagnetic polarizability

The time evolution of the magnetic configuration $\{\boldsymbol{M}\}$ is given by the Landau–Lifshitz equations:

$$\partial\boldsymbol{M}/\partial t = -|\gamma|\mu_0[\boldsymbol{M} \wedge \boldsymbol{H} + (\alpha_{LL}/M_S)\boldsymbol{M} \wedge (\boldsymbol{M} \wedge \boldsymbol{H})], \tag{20}$$

where $\gamma = -1.7 \times 10^{11}$ SI is the gyromagnetic ratio of the free electron and α_{LL}, a dimensionless damping parameter. Introducing the set of reduced quantities

$$\boldsymbol{m} = \boldsymbol{M}/M_S, \quad \boldsymbol{h}_{ext} = \boldsymbol{H}_{ext}/M_S \quad t \to |\gamma|\mu_0 M_S t. \tag{21}$$

Using the generalized demagnetizing operator introduced above, Eq. (20) can be rewritten as

$$\{\partial\boldsymbol{m}/\partial t\} = \{-\boldsymbol{m} \wedge [-\tilde{\boldsymbol{N}}\{\boldsymbol{m}\} + \boldsymbol{h}_{ext}] - \alpha_{LL}\boldsymbol{m} \wedge (\boldsymbol{m} \wedge [-\tilde{\boldsymbol{N}}\{\boldsymbol{m}\} + \boldsymbol{h}_{ext}])\}. \tag{22}$$

Linearizing this equation with respect to $\boldsymbol{h}_{ext}$ and $\delta\boldsymbol{m}$, the induced magnetization is defined by

$$\delta\boldsymbol{m} = \boldsymbol{m} - \boldsymbol{m}_0 \tag{23}$$

we get:

$$\{\partial\delta\boldsymbol{m}/\partial t\} = (-\boldsymbol{D}_1 \circ \tilde{\boldsymbol{N}} + \boldsymbol{D}_2)\{\delta\boldsymbol{m}\} + \boldsymbol{D}_1\{\boldsymbol{h}_{ext}\}, \tag{24}$$

where $\boldsymbol{D}_1$ and $\boldsymbol{D}_2$ are linear operators defined by

$$\boldsymbol{D}_1\{\boldsymbol{v}\} = \{-\boldsymbol{m}_0 \wedge \boldsymbol{v} - \alpha_{LL}\boldsymbol{m}_0 \wedge (\boldsymbol{m}_0 \wedge \boldsymbol{v})\}, \tag{25}$$

$$\boldsymbol{D}_2\{\boldsymbol{v}\} = \{-\tilde{\boldsymbol{N}}\{\boldsymbol{m}_0\} \wedge \boldsymbol{v} + \alpha_{LL}\boldsymbol{m}_0 \wedge (\boldsymbol{v} \wedge \tilde{\boldsymbol{N}}\{\boldsymbol{m}_0\})\}. \tag{26}$$

For a harmonic excitation $\boldsymbol{h}_{ext}e^{i\omega t}$, linear Eq. (24) yields a harmonic response $\delta\boldsymbol{m}e^{i\omega t}$ (ω being the reduced angular frequency). Introducing λ, the unitary vector along $\boldsymbol{h}_{ext}$ ($\{\lambda\}$ uniform), the response configuration $\{\delta\}$, generally non-uniform and non-unitary, is the solution of the following linear system:

$$(i\omega + \boldsymbol{D}_1 \circ \tilde{\boldsymbol{N}} - \boldsymbol{D}_2)\{\delta\} = \boldsymbol{D}_1\{\lambda\}. \tag{27}$$

The total magnetic moment induced in the particle by $\boldsymbol{h}_{ext}$ is

$$\boldsymbol{p}_\lambda(t) = M_S|\boldsymbol{h}_{ext}|e^{i\omega t}\int_\Omega \{\delta\}\,dx, \tag{28}$$

where the sum over Ω yields a vector in the three-dimensional space, generally non-collinear to λ. Thus, the polarizability must be defined as a 3×3 tensor, giving the component in the direction λ' of

$\boldsymbol{p}_\lambda$, which can be written as

$$\alpha(\lambda, \lambda') = \frac{1}{V}\lambda' \cdot \int_\Omega (\mathrm{i}\omega + \boldsymbol{D}_1 \circ \tilde{\boldsymbol{N}} - \boldsymbol{D}_2)^{-1} \circ \boldsymbol{D}_1 \{\lambda\}\, \mathrm{d}x, \tag{29}$$

where the scalar product is the usual scalar product in the three-dimensional space. This definition is consistent with Eq. (1) and generalizes Eq. (6).

3.3. Space average

The permeability measured on an isotropic composite is scalar. This is due to an average over all possible particle orientations inside the matrix. With the micromagnetic model, we first calculate the polarizability tensor of one representative particle, as described above, and then perform a space average to express permeability from the polarizability coefficients along the different space directions.

In the case of randomly oriented particles, the average polarizability in three-dimensional space α^0_{3D} is the trace of operator α:

$$\alpha^0_{3D} = \frac{1}{3}(\alpha_{xx} + \alpha_{yy} + \alpha_{zz}). \tag{30}$$

The complex permeability is then defined from Eq. (8), valid in the low-concentration regime ($C < 30\%$). The imaginary part is

$$\frac{\mu''}{\mu_0} = C\ \mathrm{Im}[\alpha^0_{3D}] \tag{31}$$

and can be compared to experiment. This result is used below, in the section concerning ferrite composites (where μ''/μ_0 is denoted χ'').

In the case of a non-isotropic material, the space average must be adapted. Such a material can be a textured composite or a film. For example, the films with perpendicular anisotropy studied in Ref. [4] generate magnetic domains in the form of parallel stripes with a magnetization vector oriented alternatively along z or $-z$, z being the anisotropy direction perpendicular to the film's plane (x, y) (see Fig. 1a). The alternate stripes group into well arranged regions with limited spatial extent. Considering a great number of such regions, randomly oriented with respect to each other in the (x, y) plane, and $\boldsymbol{H}_{ext}$ lying in this plane, the average polarizability in two-dimensional space α^0_{2D} is now:

$$\alpha^0_{2D} = \frac{1}{2}(\alpha_{xx} + \alpha_{yy}). \tag{32}$$

The imaginary part of the film's permeability relative to vacuum χ'' is then

$$\chi'' = \mathrm{Im}[\alpha^0_{2D}] \tag{33}$$

consistent with definition of Ref. [4]. This result is used below, in the section concerning domain modes in films.

4. Numerical simulations

The micromagnetic model described above has been implemented on computer, using specific numerical methods, and tested on two systems: domain modes in films and permeability of composites made of ferrite particles with planar anisotropy.

4.1. Discretization

Particles and regions of thin films are represented by a finite magnetic volume, regularly meshed with cubic cells (i or j: cell index). The magnetization is uniform over each cell. $\boldsymbol{m}^i_k$ is the magnetization vector of cell i at instant t_k. $\boldsymbol{h}^j_k$ is the average, instantaneous magnetic excitation, generated at cell j and instant t_k by the entire magnetic configuration $\{\boldsymbol{m}\}_k$.

The configurations $\{\boldsymbol{m}\}_k$ and $\{\boldsymbol{h}\}_k$ are $3N$ vectors with N, the number of cells of the three-dimensional mesh. Eq. (18) is discretized in the form of a matrix–vector product:

$$\{\boldsymbol{h}\}_k = \boldsymbol{C} \cdot \{\boldsymbol{m}\}_k + \{\boldsymbol{h}_{ext}\}_k, \tag{34}$$

where $\boldsymbol{h}_{ext}$ is the uniform harmonic external excitation by the electromagnetic wave. Due to the demagnetizing field which is non-local, $\boldsymbol{C}$ is a dense matrix of size $3N \times 3N$. Its coefficients are calculated as in Ref. [18], except for an average of the demagnetizing field over the volume of the target

cell (index j) where a Gaussian integration is performed [14]. This insures that $-\boldsymbol{C}$ is a correct discrete approximation of the continuous generalized demagnetizing operator $\tilde{\boldsymbol{N}}$.

The equilibrium configuration is calculated by having a given initial configuration $\{\boldsymbol{M}_i\}$ evolve in time according to equation Eq. (22) towards a stationary configuration $\{\boldsymbol{M}_0\}$ with $\boldsymbol{H}_{ext} = \boldsymbol{0}$. The time discretization of Eq. (22) follows the second-order explicit Taylor scheme:

$$\{\boldsymbol{m}\}_{k+1} = \{\boldsymbol{m}\}_k + (t_{k+1} - t_k)\boldsymbol{f}\cdot\{\boldsymbol{m}\}_{k+1/2} \tag{35}$$

with

$$\{\boldsymbol{m}\}_{k+1/2} = \{\boldsymbol{m}\}_k + (t_{k+1/2} - t_k)\boldsymbol{f}\cdot\{\boldsymbol{m}\}_k,$$

$$t_{k+1/2} - t_k = \tfrac{1}{2}(t_{k+1} - t_k),$$

$$\boldsymbol{f}\cdot\{\boldsymbol{m}\}_k = \{\boldsymbol{m}\}_k \wedge \boldsymbol{C}\cdot\{\boldsymbol{m}\}_k + \alpha_{LL}\{\boldsymbol{m}\}_k \wedge (\{\boldsymbol{m}\}_k \wedge \boldsymbol{C}\cdot\{\boldsymbol{m}\}_k, \tag{36}$$

where $\boldsymbol{f}\cdot\{\boldsymbol{m}\}_{k+1/2}$ is expanded at order 1 in $(t_{k+1} - t_k)$. The energy difference $E_{k+1} - E_k$ being simply a degree four polynomial in $(t_{k+1} - t_k)$, t_{k+1} is chosen inexpensively for each iteration so as to maximize the energy decrease $(E_{k+1} - E_k)/(t_{k+1} - t_k)$. The power dissipation, represented by α_{LL} in Eq. (36), insures convergence towards the stationary configuration $\{\boldsymbol{M}_0\}$. The optimal time step $(t_{k+1} - t_k)$ is related to d^2 (d being the unit cell dimension), which insures stability [14].

The polarizability corresponding to $\{\boldsymbol{M}_0\}$ is calculated from the solution of the linear dense system arising from discretization of Eq. (27)

$$(i\omega\boldsymbol{Id} - \boldsymbol{Y}\circ\boldsymbol{C} - \boldsymbol{X})\cdot\{\delta\} = \boldsymbol{Y}\cdot\{\lambda\}. \tag{37}$$

To solve this system, we use a standard conjugate gradient iterative method with λ alternatively along x, y and z. By summing all components of $\{\delta\}$ in one direction (x, y or z), we end up with the 3×3 polarizability tensor α defined by Eq. (29). The space average is then performed as described above to yield the permeability. This process is repeated for tens of frequencies to yield polarizability or permeability spectra.

4.2. Computer implementation

Both algorithms, equilibrium and polarizability, rest on dense matrix–vector products like Eq. (34) which normally involve handling of the order of N^2 unknowns for a mesh of N cells. To perform simulations with $N > 1000$, specific algorithms had to be developed.

In the case of a regular mesh, matrix C has a Toeplitz structure. Applying matrix C to any vector is equivalent to performing a convolution, which can be done by Fourier transform. This property greatly reduces the required number of operations and storage (proportional to $N \log N$ instead of N^2 and N instead of N^2, respectively) [13]. At present, the three-dimensional Toeplitz matrix–vector product has been implemented to calculate both equilibrium and polarizability of rectangular prism-shaped particles. In all the cases tested (up to $N = 64^3 \sim 2\times10^5$ cells on a workstation), satisfactory convergence has been observed. With the largest meshes, the required number of iterations (equilibrium or polarizability spectrum) is of at least 1000, each with a duration of the order of 1 min. These performances could be increased (e.g. by parallel computing or sub-domain calculations).

Indeed, realistic simulations often require far above 10^6 cells. The usual meshing criteria in micromagnetics requires a few cells per domain wall width ($\sqrt{A/K}$). With typical material parameters, this width is of the order of 0.1 μm. A typical polydomain particle size of $30\times30\times30$ μm leads to $N > 10^7$. The calculations presented below have been performed with a coarser mesh: the aim was simply to test the model and show that the simulations yielded qualitatively correct results.

4.3. Domain modes in films

In magnetic films made of regions with alternate stripe domains (See Fig. 1a and the discussion in Section 3.3), the magnetostatic interaction between domains gives rise to domain modes in the microwave range. An analytical model of the response of such films, validated on experimental data, is given in Ref. [4].

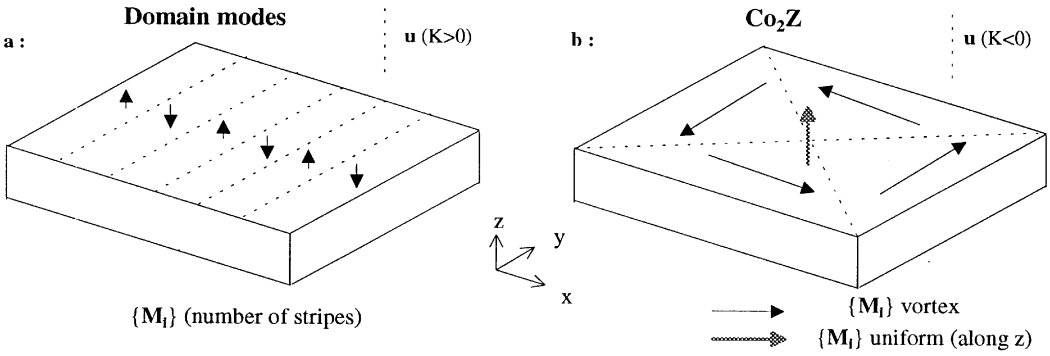

Fig. 1. Magnetization configurations used as initial conditions for numerical simulation with the micromagnetic model. In the case of a magnetic film with perpendicular anisotropy (a), the equilibrium magnetization is arranged in stripes whose width changes with film thickness; these stripes give rise to domain modes in the microwave range. In the case of a platelet-shaped particle with planar anisotropy (b), due to the exchange interaction, the particles physical size affects the equilibrium configuration and the corresponding polarizability spectrum (shown are the two initial configurations used for numerical simulations).

Finite portions of film of increasing physical size (number of stripes) have been simulated using the micromagnetic model. According to Ref. [4], a film with the following material parameters:

$$M_S = 9.1 \times 10^4 \text{ A m}^{-1},$$
$$K = 1.3 \times 10^4 \text{ J m}^{-3}, \tag{38}$$
$$A = 10^{-11} \text{ J m}^{-1}$$

and a thickness of 4.8 μm generates stripes of width around 1.2 μm. We first tried to reproduce numerically the equilibrium configuration: in this case, the micromagnetics meshing criteria are particularly stringent, the wall thickness ($\sqrt{A/K} \sim 0.03$ μm) being much smaller than the stripe width. With a coarse mesh of one cell per stripe width, smooth stripes were obtained only with initial conditions close to this expected equilibrium configuration. Large deviations from regular stripes in initial conditions or an increased number of cells (e.g., two cells per stripe width) leads to a checkered configuration, which we interpret as a signature of the mesh coarseness. The calculations were restricted to one mesh size and one initial configuration (see Fig. 1a).

The equilibrium configuration was calculated for regions with up to 64 stripes. The corresponding mesh sizes were the following:

$$N = 8 \times 8 \times 4 \text{ (8 stripes: } 9.6 \times 9.6 \times 4.8 \text{ μm)},$$
$$N = 16 \times 16 \times 4 \text{ (16 stripes: } 19.2 \times 19.2 \times 4.8 \text{ μm)},$$
$$N = 32 \times 32 \times 4 \text{ (32 stripes: } 38.4 \times 38.4 \times 4.8 \text{ μm)},$$
$$N = 64 \times 64 \times 4 \text{ (64 stripes: } 76.8 \times 76.8 \times 4.8 \text{ μm)}. \tag{39}$$

The simulated equilibrium configuration $\{\boldsymbol{M}_0\}$ is distorted on the edges, as illustrated in Fig. 2.

The polarizability tensor of an increasing number of stripes at equilibrium was simulated for different values of α_{LL}. This tensor was found diagonal (on the entire frequency range, the off-diagonal terms remained below 1% of the diagonal terms maximum) and the susceptibility was deduced using formulas (32) and (33). The results, compared to the analytical model (formula (9) of Ref. [4]) are shown in Fig. 3. For a large α_{LL} (case $\alpha_{LL} = 0.16$), the simulated spectrum has the right shape and amplitude, except for a shift towards high frequencies. This effect comes from the fact that the simulation is done for a finite region, yielding a polarizability, while the analytical calculation is representative of the infinite two-dimensional film,

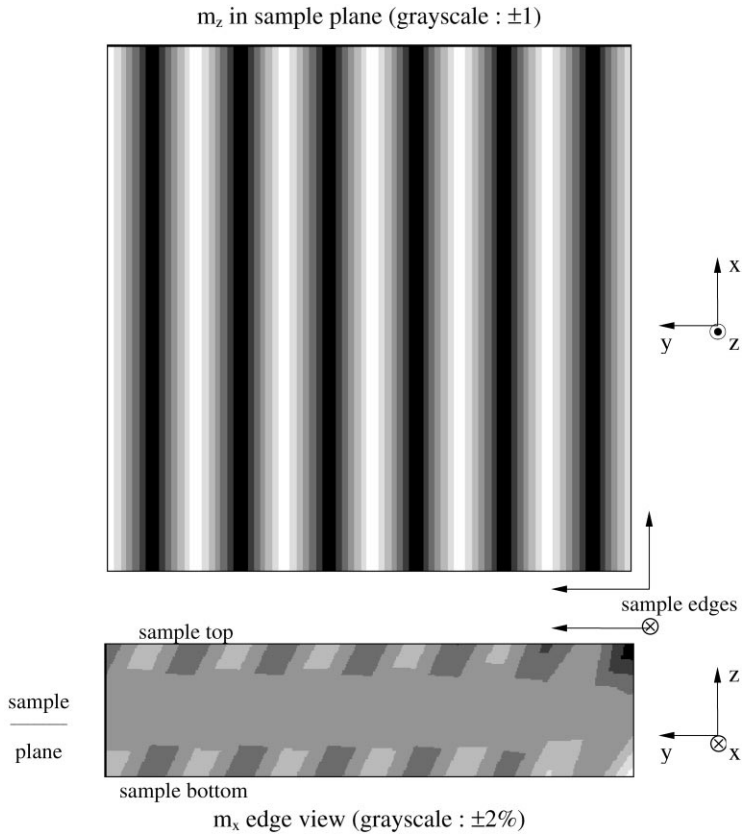

Fig. 2. Equilibrium configuration in a finite portion of film ($76.8 \times 76.8 \times 4.8$ μm; $N = 64 \times 64 \times 4$ cells). The total number of stripes in the simulated region is 64 (see text for material parameters); the area shown corresponds to a zoom at a corner of the equilibrium configuration. The initial conditions are perfect stripes (see Fig. 1a); the mesh is coarse and is one cell per stripe width. One magnetization component is shown at a time (square area: internal cross-section of the z-component in the (x, y) plane with black/white $= \pm 1$; rectangular area: external side view of the x component in the (y, z) plane with black/white $= \pm 2\%$). The simulated configuration is only slightly distorted with respect to uniform stripes along z (see right-hand side of the rectangular area: 2% maximum in terms of magnetization component along x).

yielding a susceptibility: as expected, the simulated spectrum gets closer to the analytical spectrum as the film size increases. The shift of polarizability towards high frequencies with respect to susceptibility is qualitatively accounted for by formula (6). For a small α_{LL} (case $\alpha_{LL} = 0.04$), the simulated spectrum is significantly altered with respect to the analytical spectrum. However, the α_{LL} dependence of the resonance frequencies is the same with both models.

Hence, in spite of the mesh coarseness, our simulations based on the micromagnetic model account qualitatively for the behavior of domain modes in films and could give an insight into the finite size effects in these systems.

4.4. Ferrite composites

The permeability spectrum of composites made of cobalt Z hexaferrite (Co_2Z) particles changes according to the average particle size in the composite [6]. This Co_2Z composition is known for its high permeability at high frequency [19] which stems from the planar anisotropy, constraining

magnetization motion inside a crystalline plane. The particle size effect is observed for particle sizes R in the 10 μm range. This critical size of 10 μm corresponds to the width of flat hexagonal monocrystalline Co_2Z platelets of thickness $\sim R/4$. The hard axis is perpendicular to the platelet. Particles of size greater than 10 μm are roughly isotropic aggregates of such platelets.

In order to describe the magnetic configuration change with particle size, numerical simulations were performed on idealized square platelet shaped particles with different physical sizes (width $R = 3.2$ and 32 μm; thickness $R/4$), using a coarse mesh as before. The following material parameters were considered for Co_2Z:

$$M_S = 2.7 \times 10^5 \text{ A m}^{-1},$$

$$|K| = 4 \times 10^3 \text{ J m}^{-3} \ (K < 0), \tag{40}$$

$$A = 1.2 \times 10^{-12} \text{ J m}^{-1},$$

$$\alpha_{LL} = 0.2,$$

where K represents the first anisotropy term (purely uniaxial planar anisotropy). The anisotropy axis is along z and (x, y) is the easy plane.

The simulated equilibrium configurations for two mesh sizes ($N = 32 \times 32 \times 8$ or $N = 64 \times 64 \times 16$) and two initial configurations $\{\boldsymbol{M}_i\}$ (uniform or vortex: see Fig. 1b) are shown in Fig. 4. In all four cases, the equilibrium magnetization lies in the (x, y) plane. All configuration except one (upper left in Fig. 4) are clearly vortices: such configurations are well known in simulated three-dimensional finite systems [20] or even in real mesoscopic structures [21]. Even if the mesh is too coarse to give all the details of the configurations, the difference between them lies mainly in the system's physical size:

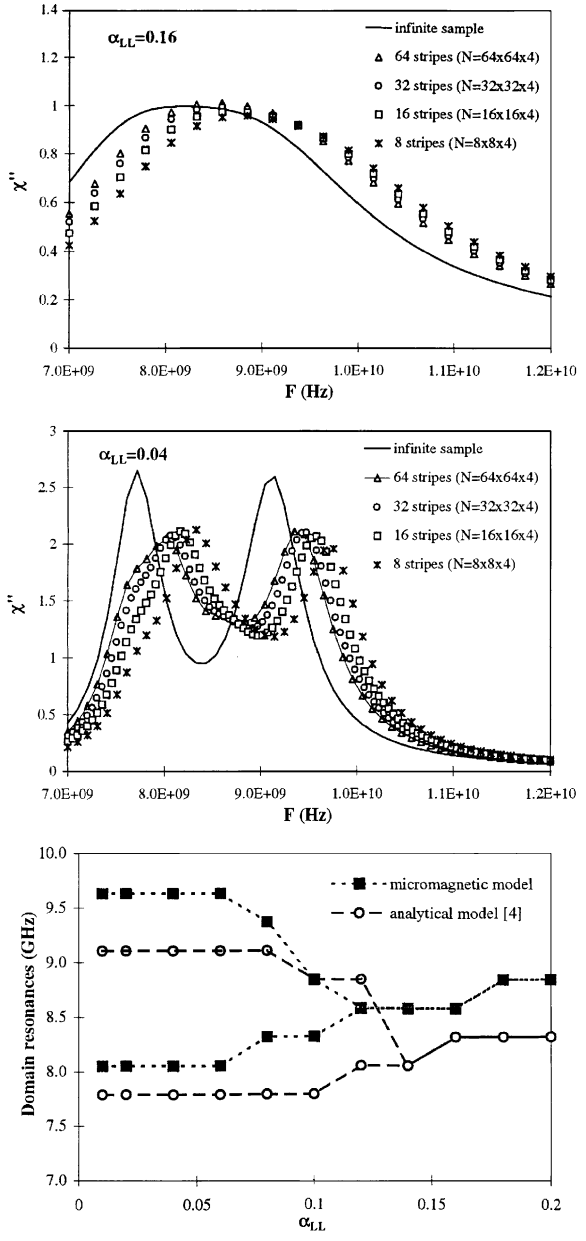

Fig. 3. Comparison of the micromagnetic model with an analytical model for domain modes in films. The microwave susceptibility spectra of films with perpendicular anisotropy have been calculated for different values of the Landau–Lifshitz damping parameter α_{LL}. Imaginary part results are shown in the two upper plots ($\alpha_{LL} = 0.16$ and 0.04; see text for material parameters): the dotted spectra correspond to simulations with the micromagnetic model (finite portions of film as in Fig. 2, of increasing physical size, i.e. number of stripes); the continuous spectra correspond to analytical calculations using formula (9) of Ref. [4] (valid for an infinite sample). The simulated spectrum tends towards the analytical one as the simulated region extends; the analytical dependence of resonance frequencies with α_{LL} is also reproduced by simulation (see lower plot).

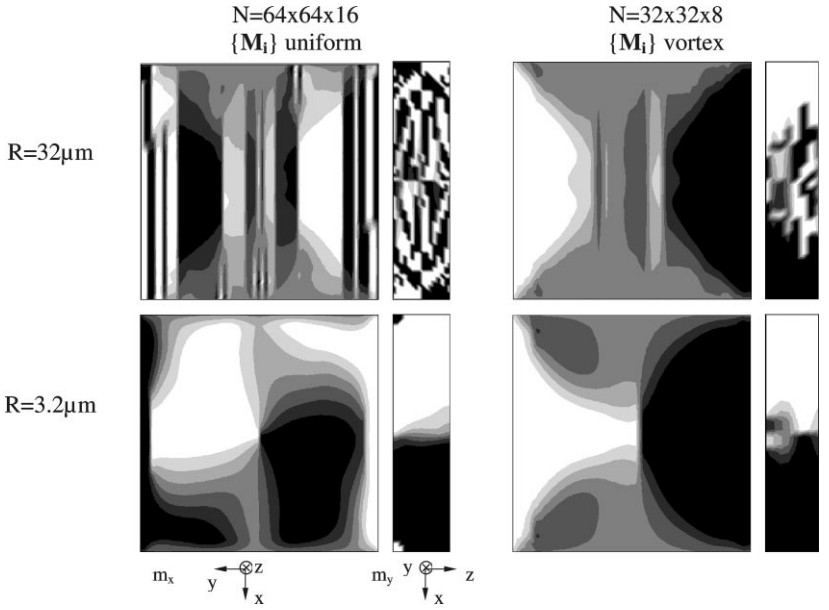

Fig. 4. Equilibrium configuration in a platelet shaped hexaferrite (Co_2Z) particle of width 3.2 and 32 μm. The simulations have been done with different initial conditions ($\{\boldsymbol{M}_i\}$ uniform or vortex; see Fig. 1b) and mesh sizes ($N = 32 \times 32 \times 8$ and $N = 64 \times 64 \times 16$; see text for material parameters). One magnetization component is shown at a time (square area: external top view of the x component in the (x, y) plane with black/white $= \pm 1$; rectangular area: internal cross-section of the y-component in the (x, z) plane with black/white $= \pm 1$). In three cases, the simulated configuration is close to a vortex. For the larger size ($R = 32$ μm), this vortex decomposes into smaller regions of opposite magnetization in the platelet's plane. These results appear qualitatively independent of initial conditions and mesh size.

for the two initial conditions and mesh sizes, the configuration grows more complex as the physical size increases from $R = 3.2$ to 32 μm.

The polarizability tensor corresponding to the two configurations with $N = 32 \times 32 \times 8$ in Fig. 4 were simulated: as before, the tensor was found diagonal. The results are shown in Fig. 5 and compared to the conventional model, using formula (7) for α and formula (4) of Ref. [3] for χ. The composite's permeability was deduced from these data, using formulas (30) and (31), and compared to experimental data. The results are shown in Fig. 6. The micromagnetic model, unlike the conventional model, yields a stronger response at high frequency, which is closer to experiment. Moreover, it renders the double peak feature of the experimental spectra, in the correct frequency range. These two peaks appear in diagonal terms of the polarizability tensor (xx and yy in Fig. 5) which indicates that this is not a simple demagnetizing effect due to particle shape but rather, a signature of the non-uniformity of magnetization inside the particle. A better agreement between calculations and experiment in Fig. 6 would require a more realistic geometry than a square prism to model these hexagonal platelet particles.

5. Conclusion

The relevance of the micromagnetic model for microwave polarizability, presented in this article, has been shown through preliminary simulations. In the case of films with stripe domains, the results agree with an analytical model of domain modes. In the case of cobalt Z hexaferrite (Co_2Z) composites, the micromagnetic model accounts for some original features of the experimental permeability

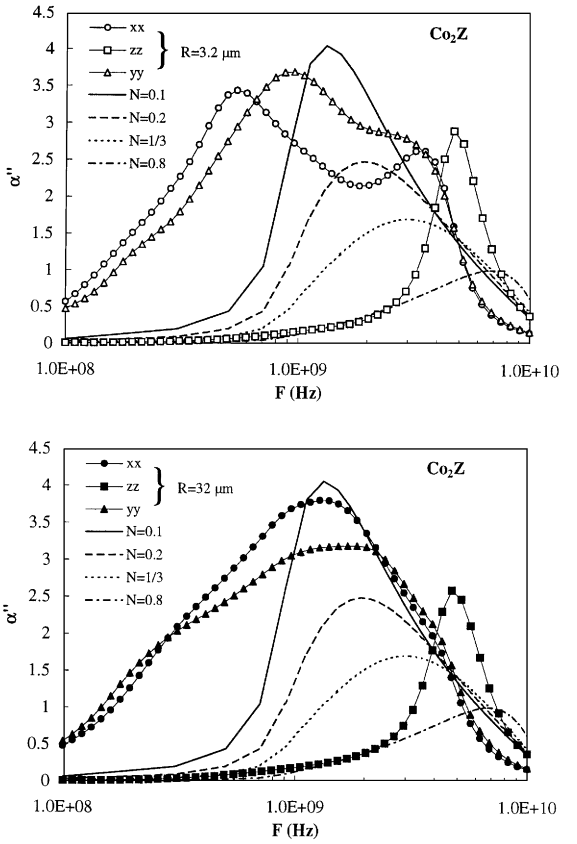

Fig. 5. Comparison between the micromagnetic model and the conventional model for particle polarizability. The system is an hexaferrite (Co_2Z) particle. The polarizability tensor corresponding to the two $N = 32 \times 32 \times 8$ configurations of Fig. 4 ($R = 3.2$ and 32 μm) have been simulated and compared to those calculated using the conventional model (with different N to account for the particle's shape anisotropy along the three space directions). Only the imaginary part of the polarizability tensor diagonal terms are plotted (off-diagonal terms are negligible). The micromagnetic model yields a stronger polarizability in the z-direction at a frequency higher than the conventional model, irrespective of N.

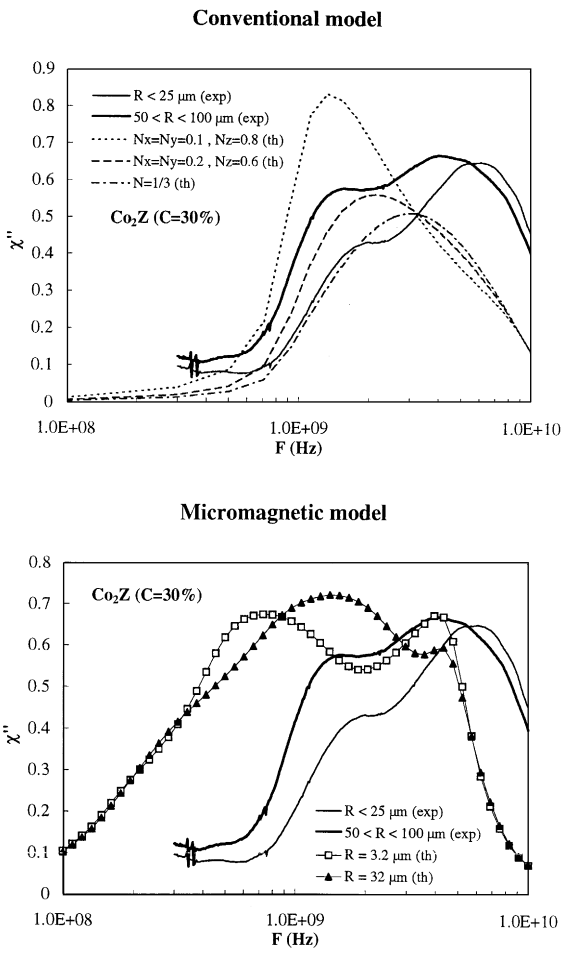

Fig. 6. Comparison between theory (conventional model or micromagnetic model) and experiment on a ferrite composite. The imaginary part of the permeability of a composite made of hexaferrite (Co_2Z) particles at $C = 30\%$ volume fraction is plotted. The experimental spectra (exp) are reproduced from Ref. [6]: they have been obtained for different mean particle sizes ($R < 25$ μm and 50 μm $< R <$ 100 μm). The theoretical spectra (th) in the upper plot has been calculated with the conventional model, for different particle aspect ratios: this model does not account for the double peak feature and for the high frequency response. The spectra simulated for a platelet-shaped particle with planar anisotropy, using the micromagnetic model, are qualitatively closer to experiment: this model yields a stronger response at high frequency, the double peak feature and a change of the spectra with particle size.

spectra that are not accounted for by the conventional model.

Beyond these qualitative results, the capacity of numerical simulations should be increased to larger number of cells in order to satisfy the usual meshing requirement in micromagnetics and verify the effect of initial conditions on the simulated susceptibility spectrum. Finally, a quantitative agreement of simulations with experiment requires also the ability to simulate complex particle shapes.

Acknowledgements

This work was carried out in the context of University Paris 13 — ONERA interdisciplinary work group on micromagnetism with L. Halpern, P. Leca, F. Alouges and L. Quivy. We are indebted to E. Flavin and F. Boust (ONERA) for their experimental work and enlightening discussions.

References

[1] G.T. Rado, R.W. Wright, W.H. Emerson, A. Terris, Phys. Rev. 88 (1952) 909.
[2] E. Schlömann, J. Appl. Phys. 41 (1970) 204.
[3] J.-P. Bouchaud, P.G. Zerah, J. Appl. Phys. 67 (1990) 5512.
[4] N. Vukadinovic, J. Ben Youssef, H. Le Gall, J. Magn. Magn. Mater. 150 (1995) 213.
[5] J. Gieraltowski, A. Globus, IEEE Trans. Magn. MAG-13 (1977) 1357.
[6] E. Flavin, F. Boust, H. Pascard, Proceedings of ICF7 in Bordeaux, France, 1996.
[7] A. Aharoni, Introduction to the theory of ferromagnetism, Oxford Science Publication, London, 1996.
[8] M.E. Schabes, H.N. Bertram, J. Appl. Phys. 64 (1988) 1347.
[9] T. Schrefl, R. Fisher, J. Fidler, H. Kronmüller, J. Appl. Phys. 76 (1994) 7053.
[10] K. Patek, A. Thiaville, J. Miltat, Phys. Rev. B 49 (1994) 6678.
[11] J. Planès, J. Appl. Phys. 75 (1994) 5698.
[12] P.-Y. Bertin, E. Flavin, S. Labbé, L. Ramanitra, F. Henry, J. Bigot, Proceedings of JCMM in Chambéry, France (1996).
[13] S. Labbé, P. Leca, C.R. Acad. Sci. Paris 327 (1998) 415.
[14] S. Labbé, Ph.D. Thesis, University of Paris 13, 1998.
[15] J.D. Jackson, Classical Electrodynamics, Wiley, New York, 1962, p. 193ff.
[16] M. Le Floc'h, J.-L. Mattei, P. Laurent, O. Minot, A.M. Konn, J. Magn. Magn. Mater. 140–144 (1995) 2191.
[17] M.J. Friedman, SIAM J. Appl. Math. 39 (1980) 14.
[18] Y. Nakatani, Y. Uesaka, N. Hayashi, Jpn. J. Appl. Phys. 28 (1989) 2485.
[19] Chikazumi, Physics of Magnetism (Wiley, New York, 1964, p. 332.
[20] M.E. Schabes, H.N. Bertram, J. Appl. Phys. 63 (1988) 1347.
[21] A. Tonomura, Adv. Phys. 41 (1992) 59.